Transmission X-ray Microscopy (TXM) Reveals the Nanostructure of a Smectite Gel

ARTICLE *in* LANGMUIR · AUGUST 2008

Impact Factor: 4.46 · DOI: 10.1021/la800986t · Source: PubMed

6 AUTHORS, INCLUDING:

Marek S. Żbik
Queensland University of Technology
56 PUBLICATIONS **413** CITATIONS
SEE PROFILE

Wayde Martens
Queensland University of Technology
215 PUBLICATIONS **4,822** CITATIONS
SEE PROFILE

Ray L. Frost
Queensland University of Technology
1,231 PUBLICATIONS **21,644** CITATIONS
SEE PROFILE

Journal of Colloid and Interface Science 435 (2014) 119–127

Contents lists available at ScienceDirect

Journal of Colloid and Interface Science

www.elsevier.com/locate/jcis

The formation of a structural framework in gelled Wyoming bentonite: Direct observation in aqueous solutions

Marek S. Żbik [a,*], David J. Williams [a], Yen-Fang Song [b,*], Chun-Chieh Wang [b]

[a] Geotechnical Engineering Centre, The University of Queensland, St Lucia, Brisbane 4072, Australia
[b] National Synchrotron Radiation Research Center, 101 Hsin-Ann Road, Hsinchu Science Park, Hsinchu 30076, Taiwan, ROC

ARTICLE INFO

Article history:
Received 13 June 2014
Accepted 1 August 2014
Available online 19 August 2014

Keywords:
Transmission X-ray microscope
Clay flocculation
Smectite flocks
Wyoming montmorillonite
Colloids
Clay gelation
Clay microstructure

ABSTRACT

Hypothesis: Particle space arrangement is a very important factor that determines the physico-mechanical properties of soil. Formations of three-dimensional (3D) structured networks within gelled or flocculated suspension may prevent clay particles and aggregates from settling under gravity force and by encapsulate water within such a network, lead to poor sludge dewatering. To better understand this phenomenon, a microstructural investigation of a smectite clay (SWy2) suspension was conducted.
Experiments: SWy-2 was diluted in water and a moderately salty aqueous solution and was studied with the aid of a synchrotron-powered transmission X-ray microscope (TXM) and cryogenic transmission electron microscope (Cryo-TEM). Observations of mutual particle arrangement in 3D spaces were conducted within a natural water environment after vitrification without drying.
Findings: A new type of micro-architecture in particle space arrangement was observed. Smectite flakes were mostly in edge-to-edge (EE) contact and formed a 3D network, confirming a "net of flakes" structural model. Clay particles form a complex and multi-hierarchic flocculated structure with characteristic cellular chained networking. Chained aggregates build cellular elements, encapsulating water inside closed voids. Increasing ionic strength results in the development of multi-hierarchic voids categories, with most water retained within nano-pores.

1. Introduction

Particle space arrangement is a very important factor that determines the physico-mechanical properties in soil. These properties play a major role in dams, footings and other engineering projects in which soil strength or permeability is crucial to the performance of a structure. As most soil mineral particles cannot be shredded by natural factors beyond a certain size, they are not present in the soil size fraction below 2 μm. Particles observed below this size limit are mostly secondary minerals that belong to the sheet silicates and are known as clays. The structure of clay-rich soils is important to a range of engineering tasks, especially those dealing with soil dewatering and stabilization. As soil structure depends on the primary particle aggregating in aqueous suspension, primary aggregating processes are the subject of increasing research interest. This study focuses on the structure of aggregates and flocks within clay-rich suspension. To avoid misunderstanding of the terms "structure" and "texture," we follow the most recent definition of "soil structure" by Osipov and Sokolov [1] as "space arrangement of all soil constituents characterized by a set of morphometric, geometric and energy parameters. It is defined by qualitative composition, quantitative ratio of all soil components and interaction between them." However, as soil macroscopic physical behavior is governed by their constitution on a microscopically small scale, we use the term "soil microstructure" in this study.

Despite numerous studies around the world, the subject is still poorly understood because of its complexity and the difficulty presented by the minute size. To enrich knowledge in this field, the present study is dedicated to investigating the microstructure of gelled smectite flocks within moderately salty aqueous uspensions. The findings from these observations may be used to improve water recovery technology primarily in mine-tailing dewatering projects.

Kaolinite, illite and smectite are the most common clay minerals in soils. Their presence in aqueous suspension is the primary cause of slow settling and water clarification problems. Clay particles are plates of flakes that are generally fine, with equivalent diameters of 200–1000 nm in kaolinites and 5–200 nm in

* Corresponding authors. Fax: +61 7 33654599 (M.S. Żbik). Fax: +886 35783813 (Y.F. Song).
E-mail addresses: m.zbik@uq.edu.au (M.S. Żbik), D.Williams@uq.edu.au (D.J. Williams), song@nsrrc.org.tw (Y.-F. Song), wang.jay@nsrrc.org.tw (C.-C. Wang).

http://dx.doi.org/10.1016/j.jcis.2014.08.004
0021-9797/

smectites with a high aspect ratio [2]. Owing to the electric charges present at the mineral surfaces (basal and edge sites) within an aqueous solution, clay particles have the ability to form complex aggregates and networks. This behavior depends on water and clay chemistry as well as the packing density of clay particles [3]. The electric charge on the mineral interface is compensated by the adsorption of cations from the solution [4]. Smectite, the most dispersed member of the clay mineral group, represents a 2:1-type layer silicate. The layered smectite structure consists of an octahedral alumina sheet sandwiched between two tetrahedral silica sheets. With the expandable structure comprising sheets carrying an excess negative layer charges are linked by weak van der Waals forces. Because of this they may easily expand in water and form nanosuspension.

Contemporary approaches to describing the behavior of dilute clay suspensions are based on the DLVO theory of colloid stability [5,6], where competing electrostatic and van der Waals forces generally determine whether particular colloidal clay suspensions will be stabilized (in sol form) or coagulated (in gel form). Chemical changes in the aqueous environment may reduce the electric charge at the mineral interface and in consequence collapse the electrical double layer and allow particles to approach each other closely enough for short-range van der Waals forces to bond them into larger aggregates. This process significantly increases the settling rate.

Given the size of clay constituents, the electron microscope (EM) was found to be the tool of choice used by scientists studying the microstructure of clays [7,8]. Development of concept about microstructure in clays can be dated back much earlier than the advent of electron microscopy methods and initiated many ideas [9–11]. The formation of a fibrillar network of particles and existence of a structural framework in sols of Wyoming was proposed in 1950s by McEwen and Pratt [12,13] The first experimental information about clay particle mutual arrangements was obtained with the advent of the transmission electron microscope (TEM) and scanning electron microscope (SEM) [3,14,15].

In terms of their settling, dewatering and filtration performance, some species of clay are quite responsive to changes in water quality, exchangeable cations concentration, flocculants type and dosage, and the treatment procedure adopted, while others remain relatively inert. The most likely cause of these differences in performance is the formation of structured networks within gelled or flocculated suspension of clay platelets may hinder particles, preventing their movement when settling in gravity force. Microstructural patterns within clay-rich suspension and sediments may not only cause settling difficulties but also in some way encapsulate water, which causes a major problem in clay-rich sludge dewatering [16–19]. The present study investigated smectite suspension microstructure in water and a medium salty aqueous environment to better understand this floccule-building phenomenon.

2. Materials and methods

The smectite used in this study was SWy2, which is a well-known Na-bentonite sample from Wyoming, obtained from the Clay Minerals Society. This bentonite is of the chemical formula $Na_{0.33}[Al_{1.67}Mg_{0.33}(O(OH))_2(SiO_2)_4]$ with high smectite content (sodium montmorillonite). SWy2 has been well described [20] and 2.5 wt% suspensions were prepared from this original clay sample in deionized (DI) water and in 0.1 M NaCl and $CaCl_2$ aqueous solutions. The suspension was sonicated 5 min with 50 power W prior to investigations. The pH was not controlled and measured in suspension at around 8.

Electrokinetic potential (Zeta potential or ζ) was measured on the clay samples using Zetasizer (NanoSeries), manufactured by Malvern Ltd., UK. Samples of diluted suspension (~0.2 wt%) were prepared from the clay fraction and inserted into a disposable measurement cell. Zeta potential in mV and electric conductivity in mS/cm were measured in DI water and 0.1 M NaCl and $CaCl_2$ salt suspensions, as described in [21–23].

X-ray diffraction (XRD) patterns were recorded with a PANalytical X'Pert Pro, multi-purpose diffractometer using Fe filtered Ca Kα radiation, autodivergence slit, 2° anti-scatter slit and fast X'Celerator Si strip detector. The diffraction patterns were recorded in steps of 0.016° 2-theta with a 0.4-s counting time per step, and logged to data files for analysis.

An EM investigation was conducted using a JEOL-2100 TEM with 200 kV accelerating potential. The SEM JEOL 6040 was used to investigate a sample coated in platinum film with accelerating voltage of 15–20 kV. For 3D imaging, the cryogenic transmission electron microscope (Cryo-TEM) was used with accelerating voltage of 300 kV. The aqueous suspension samples were vitrified into the liquid nitrogen temperature by rapid plunging samples in an environment-stable camera (stable temperature and moisture content).

The transmission X-ray microscope (TXM), which was installed on an National Synchrotron radiation Research Centre (NSRRC) synchrotron in Taiwan [24,25], proved to be an efficient instrument in the interior three-dimensional (3D) structure of nanomaterial owing to its large penetration depth and superior spatial resolution. The TXM provides two-dimensional (2D) imaging and 3D tomography at energy 8–11 keV with a spatial resolution of 50–60 nm, and has a Zernike-phase contrast capability for imaging light material that lacks X-ray absorption contrast. A photon energy of 8 keV was used to image the clay suspension for maximum X-ray absorption. The exposure time of a 2D image is from 15 s to 4 min, depending on the spot size used. By acquiring a series of 2D images with the sample rotated stepwise, 3D tomography datasets were reconstructed based on 141 sequential image frames taken in the first-order diffraction mode with azimuth angle rotating from −70° to +70° for our lateral plate specimen.

The imaging and force measurements were conducted using a Nanoscope III atomic force microscope (AFM), Digital Instruments Santa Barbara, USA, in the force mode, utilizing a scan head (JA) and standard fluid cell with a scan rate of 1 Hz used for measurements. The AFM cantilever was triangular, tipples, silicon nitride with a spherical colloidal probe (2.5 μm in diameter) purchased from NOVASCAN. The spring constant was nominal, 0.12 N/m. To record forces acting on a spring, the clay-coated flat substrate surface was displaced in a controlled manner toward and away from the colloidal probe in aqueous solutions.

Images from all microscopy studies were statistically analyzed using the Statistical Image Analyzing (STIMAN) technique [26–29], which was adopted for the study of clay suspensions. This technique can extract integrated information on sample microstructure, especially on total pore (void) space and the spread of micro-pore sizes. It contains a subroutine for estimating filtration properties from the void space parameters. Examples of the output parameters include the following: number of voids analyzed; porosity (%); total void/particle area (sq. μm); total void perimeter (μm); average diameter (μm); average perimeter (μm) and the form index (K_f), which is the ratio of platelet thickness to its diameter. Form index is 1 for perfectly round isometric particles and near 0 for string-like, elongated particles. In this study we limit the use of the STIMAN technique to obtaining statistical information about porosity, average diameter of particles and pore distribution according to their total area from 2D micrographs. The 3D STIMAN technique was also used to estimate flock size within suspension—two consequent TXM images with known rotation angle difference, these investigations were able to measuring structural elements dimension in the 3D arrangement.

TXM micrographs are the space images that carry information about the suspension layer of about 50 μm in thickness. As all samples are uniform in composition, any differences seen from consequent images photographed from different angles can provide information about the packing density of flocks. As density differs from water to particles or flocked aggregates, information about space particle packing can be transposed from 3D space images to flock dimension diagrams, as shown in the results.

3. Results and discussion

3.1. General characterization

The TEM micrograph in Fig. 1A and the AFM micrograph in Fig. 1B display the morphology patterns of the smectite sample. It represents relatively large, flexible sheets/flakes of lateral dimension ~800–1000 nm and a thickness of ~1–10 nm. The extreme thinness and flexibility of the flake-shaped particles accounts for the considerable plasticity of this mineral. Similar morphology patterns were found in earlier TEM studies [30]. The results of EM morphology studies and elemental composition show small aggregates of smectite flakes of about 1 μm in diameter. The flakes are very thin and flexible, displaying numerous wrinkles and rough, highly transparent edges, as shown in the SEM micrograph in Fig. 1B. In the AFM micrograph (Fig. 1B), smectite flakes of diameters below 1 μm form a "hand-of-card" display, with large flexible sheets spread in one fundamental unit thick steps (~1 nm). EDX analyses in Fig. 1D show typical for 2:1 smectitic Al/Si picks ratio and the presence of Na, Al, Si, Ca, and Fe elements.

The XRD results in Fig. 2 show almost pure smectite composition with a small admixture of quartz. The sample treated in the NaCl solution (Fig. 2A) displays a major 001 peak at d-space 12.31 Å, and after glycol treatment this produces a narrower and higher peak with shifts toward a larger d-space 17.16 Å. Clay treated in the $CaCl_2$ solution produces a strong and narrow peak with d-space 15.11 Å (Fig. 2B). In Na-saturated smectite, the mine 001 peak may be mobile along the d-space length depending on the moisture content, in contrast to the Ca-saturated smectite in which the mine peak is independent of the moisture content [31].

Zeta potential and electric conductivity measurements conducted in DI water and 0.1 M NaCl and $CaCl_2$ on SWy2 smectite show a gradual reduction in negative value with the increasing ionic strength of a solution.

Settling tests conducted on 2.5 wt% suspension in water and NaCl show no settling and suspension looks stable for hours, unlike $CaCl_2$ suspension, which shows coagulation and a characteristic partition between gelled fraction and clear supernatant.

3.2. Transmission X-ray microscope results

The TXM results from the smectite sample studied in water and medium salty aqueous solutions revealed anisotropy in suspension density distribution in the micro-scale (Fig. 3). Areas of larger density as observed in TXM (white) are mineral particles and aggregates which are fragments of the larger tubular super-structure (chains and ribbons) described previously in smectite suspensions [12,17].

Smectite flakes within these ribboned superstructures seem to be in EE configuration and frequently form closed cells. In Fig. 3A, chains are frequently connecting into a spanned network but distinctive linear orientation is clearly visible. The average void diameter in the observed microstructure is about 100 nm and

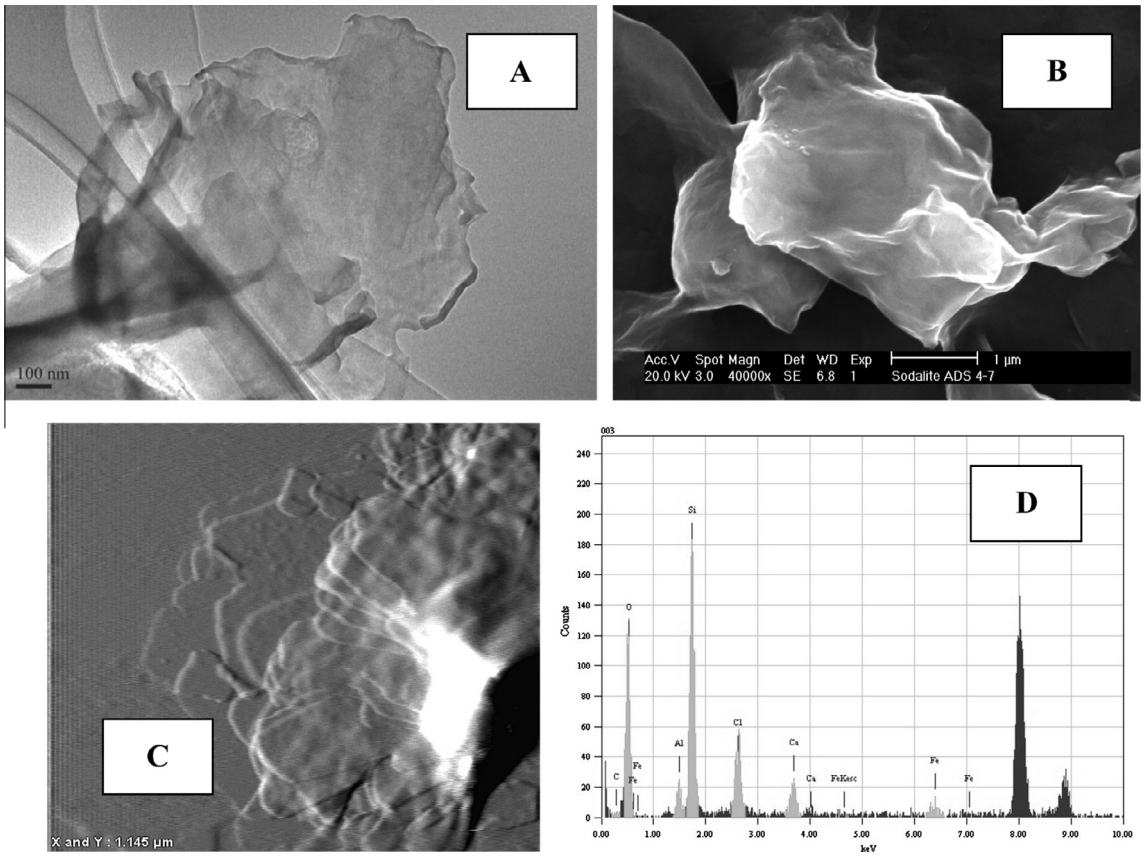

Fig. 1. (A) TEM micrograph of a smectite flexible flake. (B) SEM micrograph of a wrinkled, highly flexible smectite sheet when drying. (C) AFM micrographs show smectite flakes with one fundamental unit steps. (D) EDX spectrum shows large asymmetry of Al and Si peaks intensity.

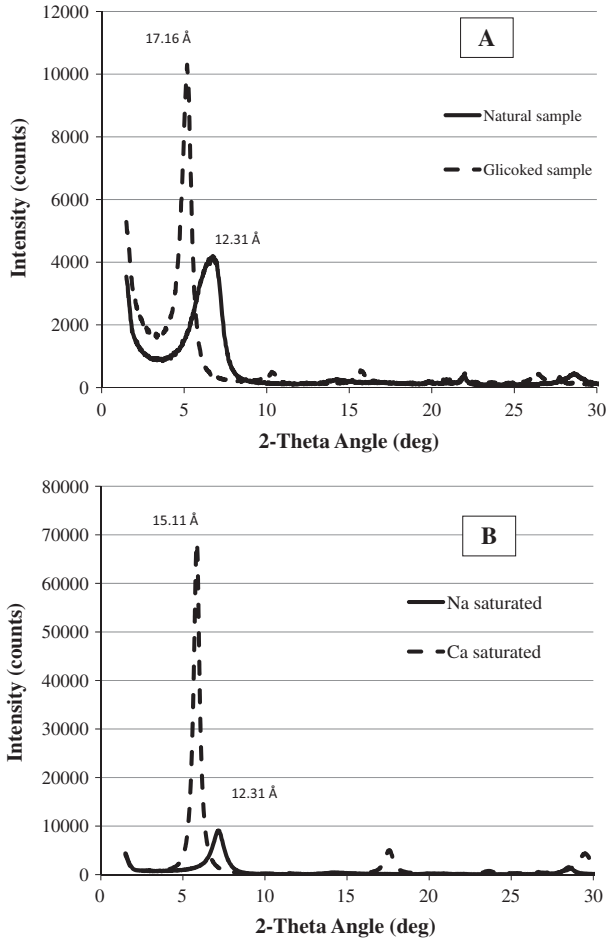

Fig. 2. The XRD pattern of the SWy-2 clay fraction sample displays smectite composition.

represents a majority intra-aggregate space. Voids between chained ultra-micro aggregates are larger and elongated. Chained micro-aggregates are often bridged and can continue in distances of a few micrometers. This gives an oriented pattern to the entire observed structure.

Surprisingly, the flocked smectite samples in water and salt solutions in the 2D TXM images show similar morphology pattern. This similarity may be due to the linear patterns within floccules. Major differences were manifested mostly in measured dimension of structural elements. Porosity measured from the area density of voids within micrograph frames was 27% in DI water, 25% in the NaCl solution and 36% in the $CaCl_2$ salt solution. The average pore diameters within the micrographs were ~78 nm in water, 82 nm in the NaCl solution and 113 nm in the $CaCl_2$ solution. Sample studied in water, shows close to Gaussian pore diameter distribution (Fig. 4) with a maximum void diameter of 250 nm. In the salt solution, voids show a multimodal distribution, which is narrower in the NaCl solution and shows three maxima of in void diameters 25, 250 and 500 nm. This distribution widens in the $CaCl_2$ solution and display maxima in voids diameters 135, 320 and 1100 nm. Most voids (by number) within flocks in water and in the NaCl solution were below 100 nm in diameter but only a small number of them had an average void diameter of 200–500 nm occupying 50–65% of the total picture frame area. Similarly, in $CaCl_{2,a}$ small number of voids ranging from ~530–1500 nm in diameter occupied 75% of the total picture frame area.

All these voids can fit within the whole range of pore dimension sizes defined in [1] for ultra-pores as less than 100 nm, and micro-pores 0.1–10 μm.

TXM observations and modal differentiation of the total void distribution in function of the voids diameter indicating that smectite particles (flakes) flocculate into a 3D network. In such a network, voids in an aqueous solution of low ionic strength (DI water) display a mostly uniform gelled microstructure. With increasing ionic strength (0.1 M NaCl), electrokinetic potential was reduced (Table 1) and particles start to coagulate into aggregates, dividing pore space into distinctive categories, intra-aggregate and inter-aggregate voids. This division increases with further rise of the ionic strength (like in 0.1 M $CaCl_2$), where particles can approach each other more closely and build denser and stronger aggregates leaving larger inter-aggregate void space on all levels of the aggregate hierarchy. This formation of a hierarchy may be a consequence of the fractal nature of clay aggregates [32–34]. In a similar way, the voids hierarchy in flocked smectite slurries may also follow the fractal low [34] but larger statistical data may be needed to confirm this assumption; investigations in this matter are in progress.

The 3D TXM computer reconstruction models and in 3D micrographs like shown in Fig. 5 give more information about the microstructural arrangement of smectite flakes and flocks (3D anaglyphs available in online).

Flocks morphology in water and in the NaCl solution are similar and display uniform gelling, where individual smectite flakes and ultra-aggregates of submicron sizes build cells, which may be the first level of the structural hierarchy. The observed primary cellular structural elements were up to 1 μm in diameter and formed chains (Fig. 5A and B), which may be the second element in the structural hierarchy. On this level, the structure displays a strong linear chain orientation, which seemed to form plaits as the third observed element in the structural hierarchy. Plaits made of chain benches may form a super-structure of column-like elements of a few microns in diameter. These structural elements on all the hierarchy levels look similar in DI water and NaCl with a little smaller cellular and chains diameter were observed in NaCl solution.

The smectite sample in $CaCl_2$ (Fig. 5C) suspension displays a lesser-order in structural elements orientation and much broader diameter distribution of these structural elements (particles, their aggregates and voids). The cellular voids are less regular in morphology and display a broad range of shapes and diameters with most primary voids below 400 nm. Short chains constituted of more compacted aggregates and a population of large and elongated inter-aggregate voids can be commonly observed.

The particle/flock dimension, calculated from TXM stereo images using STIMAN technique, gives interesting comparative data, as shown in Fig. 6. This graph shows that the flock dimension in the NaCl solution is smaller (median value 312 nm) than in the $CaCl_2$ solution (median value 483 nm). The flock dimension range is wider in the $CaCl_2$ solution (3.4 μm) than in the NaCl solution (2.35 μm). The slope is similar in both salt solutions. About 10% of measurements confirmed particles/flocks below 100 nm in diameter in the NaCl solution when the same portion of particles/flocks in the $CaCl_2$ solution was twice as large and below 200 nm in diameter.

The slope looks low in both solutions, for particles below 200 nm in diameter, which may testify to primary coagulation from individual particles and aggregates. Larger slope value, between 200–2000 nm, may indicate a wide range of flock diameters in this division. Visible undulations on size cumulative curves in Fig. 6 may indicate the hierarchic composition of flocks.

3.3. Cryogenic transmission electron microscope results

The resolution in TXM micrographs is about 60 nm or even lower due to particle movement during the relatively long exposure time when the picture was captured (60–240 s). This makes

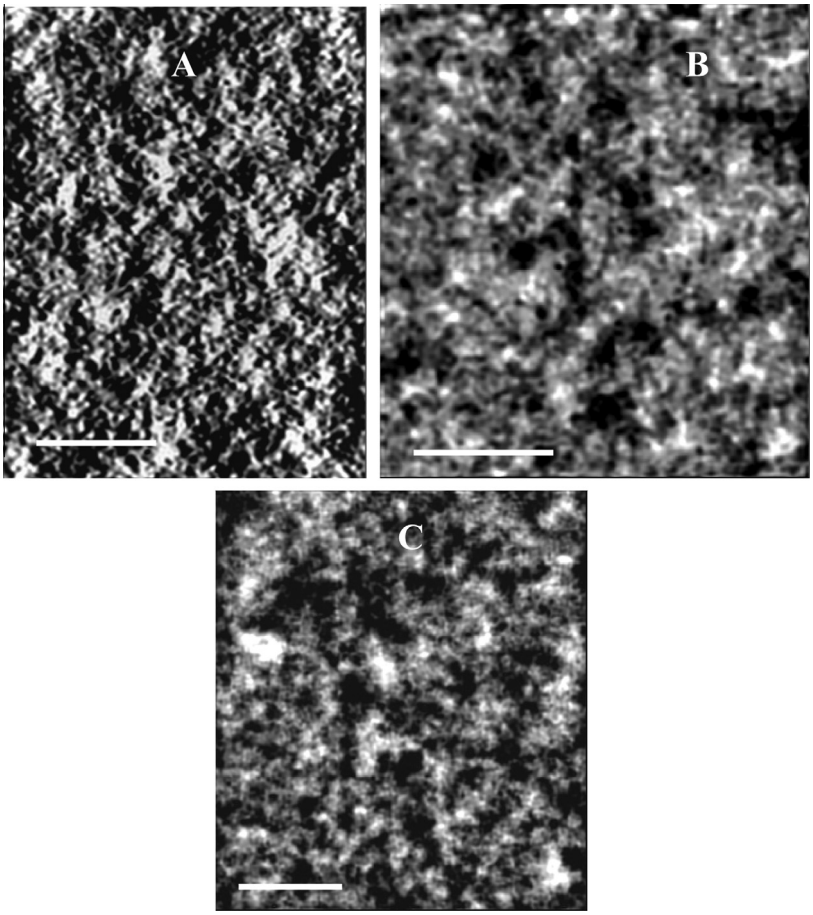

Fig. 3. A 2D TXM micrograph of the SWy-2 Wyoming smectite in: (A) DI water, (B) NaCl 0.1 M solution and (C) $CaCl_2$ 0.1 M solution; scale bars 1 μm.

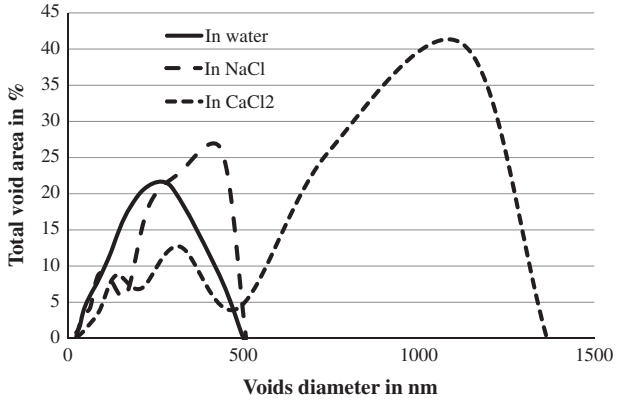

Fig. 4. The total area distribution of voids accordingly to their diameter, calculated using STIMAN technique from TXM micrographs of Swy-2 smectite in: (A) DI water, (B) NaCl 0.1 M solution, (C) $CaCl_2$ 0.1 M solution.

it, in many instances, difficult to judge from the micrographs more detail about contact between smectite flakes within aggregates, which form the basic structural elements in gelled clay suspension.

For more detail about flock morphology and microstructure in high resolution, we observed vitrified suspensions using Cryo-TEM followed by computer 3D reconstruction. Fig. 7 displays the 3D reconstructed micrographs of 2.5 wt% Swy-2 smectite suspension in aqueous salt solutions (3D anaglyphs available in online).

The average equivalent diameter of particles measured in DI water and NaCl was, between 20 and 30 nm, respectively. Their

Table 1
Zeta potential (ζ), electric conductivity (E_c) in mS/cm and average equivalent diameter (D) in nm of smectite particles in DI water. 0.1 M NaCl and 0.1 M $CaCl_2$.

	ζ (mV)	E_c in (mS/cm)	D (nm)
DI water	−61.4	0.00144	18
0.1 M NaCl	−43.5	12	27
0.1 M $CaCl_2$	−12.3	23.1	32

section area occupied 1.3–2% of the total frame surface, and the form coefficient ($K_f = 0.2$) was low (0 – for elongated string-like particles, 1 – for circular-shape particles). The magnified micrograph fragment in Fig. 7A shows smectite flakes clearly displaying a flocculated micro-structure; individual smectite flakes form a voluminous space network in which most platelets connect in edge-to-edge (EE) contact. All flake-like particles in this micrograph are between 50–500 nm in the lateral dimension and a few nm thick. They form chains of randomly oriented flakes making closed loops, which may lead to the formation of cellular elements. Such EE-contacting platelet particle configurations may occur due to competition between highly repulsive electrostatic forces between a highly negative charge on the basal surfaces of smectite flakes and attractive van der Waals forces between particle edges [35]. So each following flake tends to lie in a significantly different angle toward all neighbor flakes and forms zigzagging chained aggregates. As shown in Fig. 7A, the flakes make such associations despite their differences in lateral diameter. In this micrograph, large platelets form coagulated aggregates, zigzagging near the micrograph center, where platelets up to 0.5 μm form a ribbon-like short chain. Similarly, much smaller coagulated flakes

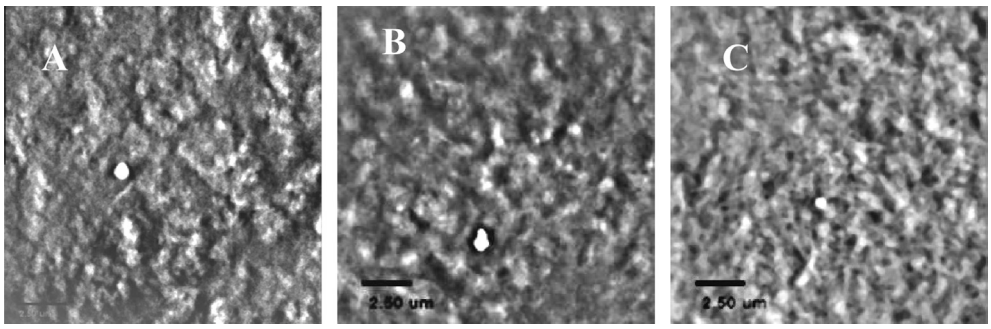

Fig. 5. TXM 3D micrographs from the SWy-2 Wyoming smectite in: (A) DI water, (B) NaCl 0.1 M solution and (C) $CaCl_2$ M solution; scale bars 2.5 μm.

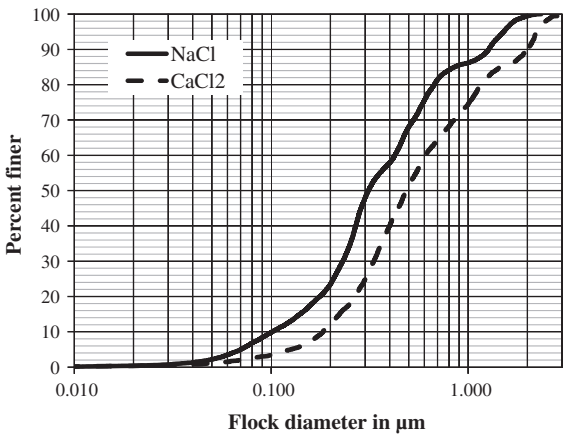

Fig. 6. Comparison of the flock diameters calculated from TXM 3D images of the SWy-2 smectite in the NaCl 0.1 M and $CaCl_2$ 0.1 M solutions.

of ~100 nm form a zigzagging loop, as displayed in this micrograph on the left-hand side pointed by an arrow.

In the $CaCl_2$ solution, smectite flakes were much thicker as they consist of a larger number of aggregates of various sizes, which were associated in face-to-face (FF) orientation. They connect with other similar aggregates, predominantly in EE contact, and build cellular elements and chains (Fig. 7B). The average equivalent diameter of particles was 32 nm, their sections occupied 3.1% of the total frame area and their form coefficient ($K_f = 0.3$), was significantly larger than in water, and still indicate predominantly largely elongated flakes. Chains consisted of parallel sandwiched flakes (tactoids) connected with similar flakes mostly in EE orientation with much less EF particle orientation. No zigzagging flocks were observed and thicker chains, by engaging a larger number of particles, leave more empty space within inter-aggregate voids.

Statistical analyses of Cryo-TEM images such as those shown in Fig 7, in water and salt solutions obtained using STIMAN technique are shown in Fig. 8. The analysis shows that particles in the Swy-2 sample represent at least a three-modal distribution, which is consistent with the structural hierarchy observed. In water, particles were smaller and peaks maxima can be found in order of the equivalent diameter 15 nm, 24 nm and 45 nm. In the NaCl solution, particles became larger with first maximum of the equivalent diameter near 24 nm, second 36 nm and third 54 nm. The largest aggregates were observed in the $CaCl_2$ solution, where maxima of different levels of particle aggregate hierarchy show peaks of 25 nm, 40 nm and 100 nm, which indicate particles twice as large as in NaCl solution. In all studied solutions, the third peak congregated majority (by surface area) of particles total area within the micrograph frame.

3.4. Atomic force microscope results

Direct measurements of forces acting between smectite-coated surfaces were measured using an AFM within Na- and Ca-salt aqueous solutions and plotted in Fig. 9. Results show that there was a long-range repulsion between smectite particles, a quasi-exponential decay of the force, and no adhesion between particle surfaces. The long-range repulsive forces for smectite in water and in the NaCl salt solution have been detected from a relatively long distance of 800–1000 nm of the surface separation, whereas

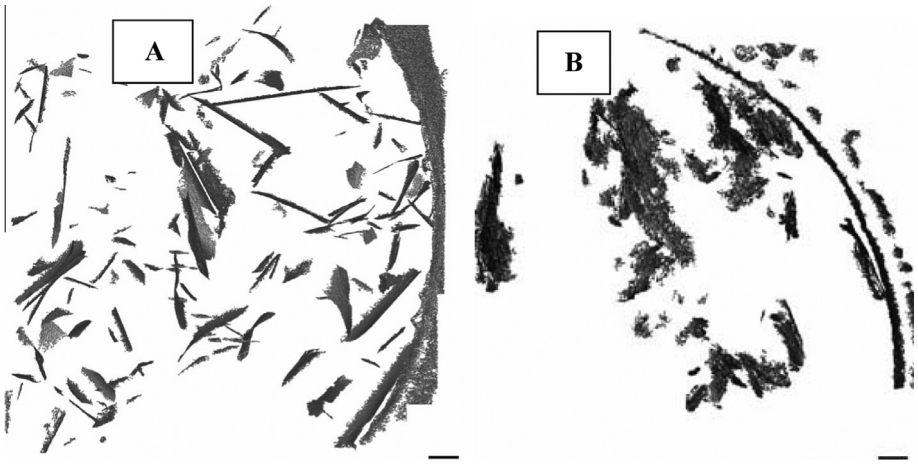

Fig. 7. 3D micrographs showing the space arrangement of smectite particles in an aqueous environment (scale bar 100 mn), as observed in the Cryo-TEM. (A) in 0.1 M NaCl, (B) in 0.1 M $CaCl_2$.

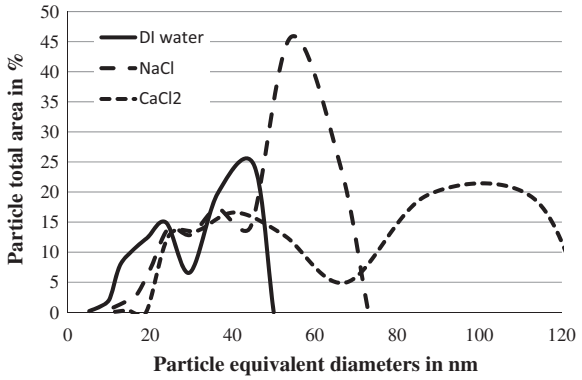

Fig. 8. Total area distribution of particles according to their lateral diameter calculated using STIMAN technique from Cryo-TEM micrographs of Swy-2 smectite, in DI water, in NaCl 0.1 M solution, and in $CaCl_2$ 0.1 M solution.

for smectite in $CaCl_2$ solution the repulsive forces were detected from a distance of ~400 nm. These numbers correspond to the aggregate dimensions observed in the TXM 3D reconstructions, as well as the 2D TXM micrographs.

Interestingly, there is little difference in forces acting between Na-smectite particles in water and in the 0.1 M NaCl salt solution, which may be because the smectite studied was Na-montmorillonite with a majority of sodium cations in exchangeable complex composition. The observed aggregate microstructure in water and NaCl was also alike. The force curve representing measurement results in the $CaCl_2$ salt solution shows a repulsive force acting from much shorter distances. The steeper curve slope in consequence was evidence of stronger forces acting in a short distance of particle separation in comparison with samples in the DI water and in the NaCl solution. Data from AFM measurements clearly confirm the existence of long-range, exponentially decayed repulsion, which looks similar to the double-layer interaction. According to Chan, Pashley and White [39], the maximum force felt is more likely related to the amount of charge on the surface, while the slope of the exponential decay at large separation distance is more related to the Debye length. However such long-range forces are hundreds of times larger than may be expected and cannot be explained on the basis of the Debye length only and was suggested having rather steric origin [17]. The measured repulsive forces may in fact represent structural network resistance against

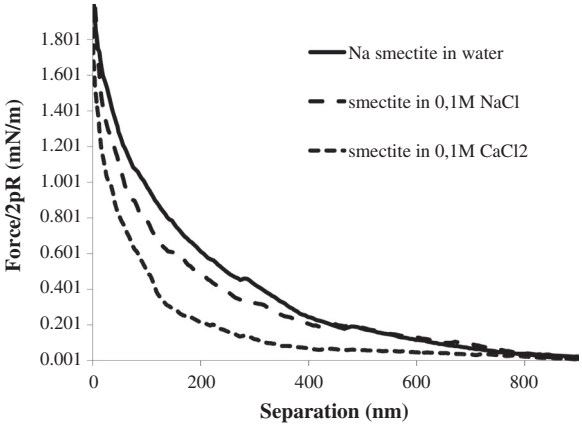

Fig. 9. Force versus separation curves obtained from AFM measurements for the interaction between Swy-2 particles on approach.

compression when smectite-coated surfaces approach each other in AFM measurements. These distances were also consistent with the dimensions of primary aggregates observed by the TXM method.

3.5. Discussion of the possible mechanism of the structure-building phenomenon

Nano-size particles are the most likely cause of this structure-building phenomenon [36]. It was found that a concentration of only 1–1.5 vol.% of nano particles is required to produce a space-filling, gel network. The presence of extremely small particles in a suspension, which is associated with smectites as observed in TEM, our morphology characterization, and STIMAN calculation, may enhance flocculation of the sample. It has been observed [37,38] that larger particles were arrested within a voluminous network of nano-clays in gelled suspension or flocks. The consequence of reducing the zeta potential within dense, clay-rich suspension is the generation of a gel with a high water-holding capacity. Within fractions containing particles of diameters less than 200 nm, suspended in 0.1 M NaCl solution, gelatin was instantaneous. Such gelled suspensions are most likely preventing particles from free settling.

From our TXM results on smectite clay suspension (SWy2), in water and in the NaCl solution, we found that 10% of particles have approximately 100 nm dimension, which placed them within nano-size particles. In the $CaCl_2$ solution, particles build larger aggregates and only about 3% fall into 100 nm size, which is enough for initiating spontaneous and almost instant flocculation within suspension. About 10% of the particles have a dimension below 200 nm, which also triggers almost instant flocculation in the salt solution. Thus, our samples, under a size fraction condition, did have the ability to form a space network and subsequently gels.

Though this structure-building phenomenon has been studied in numerous contributions, it is still poorly understood in colloid science. It is also affecting electrokinetic phenomena, where particles involved lose their mobility within suspension. Such an effect, virtually unknown in colloid science, was described by Dukhin [40] when observing clear transformation from sol to gel in dilute carbon nano-tubes suspension during electroacoustic measurements.

The mechanism responsible for the observed structure formation in aqueous suspension of dispersed smectite has been observed before [12,13] and may originate of competition between repulsive electric repulsion forces and attractive van der Waals forces as predicted by DVLO theory. Smectite flakes carry high electric potential as the zeta potential measurements show values of −61 mV in DI water and −44 mV in NaCl solution (Table 1). The flakes experienced strong electric repulsion forces when approaching each other in FF orientation.

The high particle aspect ratio makes edge surface contribution toward the total surface area insignificant. The small surface area of smectite thin flake edges causes relatively low electrostatic repulsion in EE particles orientation. Therefore, the van der Waals attractive forces may prevail and EE contacts between smectite thin flakes become favorable in such a colloidal system. In such an arrangement, particle forms spanned a 3D network of maximum space between particles. Such a network stays stable as platelets support each other with electrostatic force and their own flake elasticity against a much weaker gravity force. In effect the suspension in which such a network was formed resists settling.

Larger aggregates mostly in FF-oriented sheets observed in the $CaCl_2$ solution in Fig. 8B display in higher magnification face to edge (FE) coagulation contacts within aggregates. Distances up to 15–45 nm were measured between individual parallel-oriented flakes which build tactoid. Such aggregate microstructure was the result of a relatively lower zeta potential (−12.6 mV). In such

close proximity between platelets, where observed in Cryo-TEM micrographs, contacts were FF, EF and EE. Flakes within coagulated aggregates appeared to be in FF contact, in a similar way to that proposed by Weiss and Frank [41] in the "Bander-model."

The nature of the observed large-scale flake orientation through full suspension in DI water, and the Na and Ca salt solutions is not yet clear but may originate from the newly discovered electromagnetic interaction between clay platelets, similar to that displayed in liquid crystals. This effect in clay suspension was recently described [42–47], where the liquid–crystalline character was evidenced by polarized light microscopy in small-angle X-ray scattering observations. These experiments on smectite clay-based gel samples revealed strong positional and orientation orders of the particles, proving unambiguously the nematic character of the gel and thus clearly suggesting the need to revise Goldshmidt's [11] old "house of cards" structure model with the "net of flakes" model described here. Having this conclusion in mind, this general description of the behavior of smectite clay particles within aqueous suspension must be taken into account and is worthy of further study as a possible industrial application is likely to follow.

4. Conclusions

The arrangement of the pores between micro-particles is very important in determining the physical and mechanical parameters of soils and soil slurries. These parameters play a major role in dams, footings, colloidal stability, and the dewatering of soil slurries.

The hypothesis is that the formation of structured networks within a gel or flocculated suspension of clay particles hinders the deformation of particles and encapsulates water within the cellular structure. This is the prime cause of a suspension's resistance to settling and dewatering, particularly for clay mineral-rich slurries [1–4]. Despite much effort being paid to micro-structural studies worldwide, the settling and dewatering of soil slurries remains poorly understood. This hypothesis was inspired by the early work of McEwen [12,13], in which the formation of a three-dimensional particle network within a montmorillonite suspension was predicted from experimental results.

The current study found the following:

1. The morphology of smectite particles resembled flexible flakes a few nm to μm in diameter. These particles, spontaneously from a three-dimensional framework when dispersed in an aqueous solution.
2. A new pattern of particle networking was observed, in which clay flakes in edge-to-edge contact formed voluminous, rimmed chains zigzagging in 1–3 μm long twisted strings. This peculiar structural arrangement of smectite flakes formed spiraling short chains known as ribbons.
3. This particle networking led to the formation of a light gel. A new micro-structural model of a "**Net of Flakes**" of flocculated smectite was proposed. The proposed model is based on direct observations of the clay suspension in an aqueous solution, using X-ray and electron microscopes.
4. The light gel can be distinguished from a soil suspension by the presence of a clear supernatant layer. The light gel can be inert like the soil suspension and unlike the high viscosity gel that resembles a viscous paste.
5. Porosity measured from TXM micrographs showed an almost uniform void distribution within the gel in a low ionic strength solution. Increasing ionic strength results in the decay of pore uniformity and the development of hierarchic voids. The phase separation became more apparent when the ionic strength of the solution increased.
6. The water-encapsulating voids observed within the gel were mostly well below 1000 nm in diameter, and most of the water entrained within the network was immobilised.
7. Large micro-aggregates were observed in $CaCl_2$ solution, in which the clay platelets appeared to be arranged in face-to-face configurations, with edge-to-face coagulation contacts within the tactoids.

These findings appear to confirm the formation of three-dimensional structured networks within a gel or flocculated suspension, which may prevent the clay particles and aggregates from settling under gravity and lead to poor dewatering. In this study, the three-dimensional arrangement of the clay particles was observed in water and within moderately salty (NaCl) aqueous solution. The clay micro-aggregate flakes were arranged in a spanned network forming an elastic framework, mostly or exclusively having edge-to-edge contacts. These smectite flakes were not in parallel, but were twisted toward each other and formed zigzagging bent chains. This finding supports the proposed model of a "net of flakes" as a best fit to observations made of the smectite-rich suspensions. The high content of nano-particles in the smectite suspensions may enhance flocculation and be an important factor in the formation of the observed structural arrangement. The network remained stable because the suspension resists settling due to the platelets supporting each other against the much weaker gravity force. Smectite ultra-micro aggregated flakes (nano-clays) were small in water and produced larger aggregates in the salt solution, with the average particle equivalent diameter being ~18–27–32 nm in deionised water–NaCl–$CaCl_2$ solutions, respectively.

The observed micro-structural model was closely related to the house-of-cards model proposed by Goldshmidt in 1926 [11], but remarkably different. Goldshmidt proposed that for undisturbed and young clay sediments, the flaky clay minerals are arranged in a "house-of-cards" structure with edge-to-face contacts. In the proposed model, because of the high aspect ratio of the smectite flakes, competition between electrostatic repealing forces and attractive van der Waals forces cause the observed platelet arrangement.

The proposed model differs from the "house-of-cards" model because it applies to an aqueous suspension rather than a sediment. It represents the first stage of phase separation (dewatering), in which the water parts from the mineral phase. The suspension forms a weak, unstable gel, in which the particles resist settling.

The proposed "net of flakes" model also differs from the "honeycomb" structure proposed by Terzaghi in 1925 and Casagrande 1932 [9,10], since a complex, non-uniform, multi-hierarchic flocculated structure, with characteristic cellular chain networking is involved. The observed chained, ultra-micro aggregates build cellular structural elements that are up to 1 μm in diameter in water and NaCl solution. These cells enclose the aqueous solution. In $CaCl_2$, these structural elements were up to 400 nm in diameter and more robust, which may result in a stronger force.

The water-encapsulating voids observed within the gel were mostly well below 1000 nm in diameter, and most water retained within the network was immobilised. Despite the broadening of the larger pores with increasing solution ionic strength, most of the pore water was likely entrained within the nano-pores. This finding explains why dewatering of such suspensions is a complex and difficult task. Attempts to destabilise the network to remove water lead to the mobilization of the nano-clay particles, which may instantly rebuild the gel. Larger micro-aggregates were observed in the $CaCl_2$ solution. These were arranged in parallel and are of low density, with 15–45 nm water layers between flakes. The aggregates appeared to have edge-to-edge contacts.

Further investigation of the proposed model will focus on the structural transition of the smectite suspension from a low viscosity gel to a stable, high viscosity gel. The understanding gained may lead to the development of a comprehensive model of clay suspension behavior. Such an understanding is important in facilitating faster settling of particle aggregates, dewatering and water clarification, which has important implications for the management of clay mineral-rich mine tailings.

Acknowledgments

This work was supported by the Australian Synchrotron Research Program (ASRP) and partly funded by the ACARP Project C20047. The authors acknowledge the facilities, and the scientific and technical assistance of the Australian Microscopy & Microanalysis Research Facility at the Centre for Microscopy and Microanalysis, The University of Queensland. Elite Editing thanks for professional service in spell check, grammar and editing article text.

References

[1] V.I. Osipov, V.N. Sokolov, Proceeding of second Annual International Confernce on Geological & Earth Science (GEOS) (2013) 576 (in RUSS).
[2] M. Zbik, R.St.C. Smart, Clays Clay Miner. 46 (2) (1998) 153–160.
[3] F.A. Bowles, Science 159 (1968) 1236–1237.
[4] H. Van Olphen, An Introduction to Clay Colloid Chemistry, Interscience Publishers, New York, 1963.
[5] B.V. Derjaguin, L.D. Landau, Acta Physicochim. URSS 14 (1941) 633–652.
[6] E.J.W. Verwey, J.T.G. Overbeek, The Theory of Stability of Lyophobic Colloids, Elsevier, Amsterdam, Netherlands, 1948.
[7] P. Smart, N.K. Tovey, Electron Microscopy of Soils and Sediments: Techniques, Clarendon Press, Oxford, 1982.
[8] M. Żbik, R.St.C Smart, G.E. Morris, J. Colloid Interface Sci. 328 (2008) 73–80.
[9] K. Terzaghi, Erdbaummechanik auf BodenphysikalischerGrundlage, Franz Deuticke Press, Leipzig, 1925.
[10] A.J. Casagrande, Boston Soc. Civil Eng. 19 (1932) 168–208.
[11] V.M. Goldshmidt, Nord. Jordbrugsforsk 4–7 (1926) 434–445.
[12] M.B. McEwen, Am. Mineral. 35 (1950) 166–172.
[13] M.B. McEwen, M.I. Pratt, Trans. Faraday Soc. 53 (1957) 535–547.
[14] R. Pusch, Clay Microstructure, National Swedish Building Research, Document D8, 1970.
[15] N.R. O'Brien, Clays Clay Miner. 19 (1971) 353–359.
[16] L.S. Kotlyar, B.D. Sparks, Y. LePage, J.R. Woods, Clay Miner. 33 (1998) 103–107.
[17] M.S. Zbik, W. Martens, R.L. Frost, Y.-F. Song, Yi.-M. Chen, J.-H. Chen, Langmuir 24 (2008) 8954–8958.
[18] G.E. Morris, M.S. Żbik, Int. J. Miner. Process. 93 (2009) 20–25.
[19] M.S. Żbik, Y.-F. Song, R.L. Frost, Ch.-Ch. Wang, Minerals 2 (2012) 283–299.
[20] H. Van Olphen, J.J. Fripiat, Data Handbook for Clay Materials and Other Non-Metallic Minerals, Pergamon Press, Oxford, UK, 1979. 183.
[21] R.J. Hunter, Zeta Potential in Colloids Science, Academic Press, NY, 1981.
[22] J. Lyklema, Colloids Surf., A: Physicochem. Eng. Aspects 222 (2003) 5–14.
[23] M. Minor, A.J. van der Linde, H.P. Leeuwen, J. Lyklema, J. Colloid Interface Sci. 189 (1997) 370–375.
[24] D. Attwood, Nature 442 (2006) 642–643.
[25] G.C. Yin, M.T. Tang, Y.F. Song, F.R. Chen, K.S. Liang, F.W. Duewer, W. Yun, D.H. Ko, H.-P.D. Shieh, Appl. Phys. Lett. 88 (2006). 241115-1–241115-3.
[26] Y.M. Sergeev, G.V. Spivak, A.Y. Sasov, V.I. Osipov, V.N. Sokolov, E.I. Rau, J. Microsc. 135 (1983) 1–12.
[27] Y.M. Sergeev, G.V. Spivak, A.Y. Sasov, V.I. Osipov, V.N. Sokolov, E.I. Rau, J. Microsc. 135 (1983) 13–24.
[28] V.N. Sokolov, D.I. Yurkovets, O.V. Ragulina, V.N. Mel'nik, Bull. Russ. Acad. Sci. Phys. 68 (2004) 1491–1497.
[29] V.N. Sokolov, O.V. Razgulina, D.I. Yurkovets, M.S. Chernov, J. Surf. Invest. 1 (4) (2007) 417–422.
[30] H. Beutelspacher, H.W. van der Marel, Atlas of Electron Microscopy of Clay Minerals amd their Admixtures. A Picture Atlas, Elsevier Publishing Company, Amsterdam-London_New York, 1968.
[31] E. Ferrage, B.L. Lanson, B.A. Sakharov, V.A. Drits, Am. Mineral. 90 (2005) 1358–1374.
[32] Li.-M. Zhang, Colloids Surf., A: Physicochem. Eng. Aspects 202 (2002) 1–7.
[33] Yongfu Xu, Xiaohe Xia, Mech. Res. Commun. 33 (2006) 206–216.
[34] M. Benna-Zayani, A. Mgaidi, M. Stambouli, N. Kbir-Ariguib, M. Trabelsi-Ayadi, J.L. Grossiord, Appl. Clay Sci. 46 (2009) 260–264.
[35] A. Dathe, S. Eins, J. Niemeyer, G. Gerold, Geoderma 103 (2001) 203–229.
[36] D.Y.C. Chan, R.M. Pashley, L.R. White, J. Colloid Interface Sci. 77 (1980) 283–285.
[37] L.S. Kotlyar, B.D. Sparks, R. Schutte, Clays Clay Miner. 44 (1) (1996) 121–131.
[38] L.S. Kotlyar, B.D. Sparks, Y. LePage, J.R. Woods, Clay Miner. 33 (1998) 103–107.
[39] M.S. Żbik, D.J. Williams, Y.-F. Song, Ch.-Ch. Wang, Smectite clay flocculation structure the direct observation in moderate concentration salt solutions (submitted for publication).
[40] A.S. Dukhin, J. Colloid Interface Sci. 310 (2007) 270–280.
[41] A. Weiss, R. Frank, Naturforsch 16 (1961) 141.
[42] E. Paineau, I. Dozov, I. Bihannic, Ch. Baravian, M.-E.M. Krapf, A.-M. Philippe, S. Rouzière, L.J. Michot, P. Davidson, ACS Appl. Mater. Interfaces 4 (2012) 4296–4301.
[43] L.J. Michot, Ch. Baravian, I. Bihannic, S. Maddi, Ch. Moyne, J.F.L. Duval, P. Levitz, P. Davidson, Langmuir 25 (2009) 127–139.
[44] E. Paineau, I. Dozov, A.-M. Philippe, I. Bihannic, F. Meneau, Ch. Baravian, L.J. Michot, P. Davidson, J. Phys. Chem. B 116 (2012) 13516–13524.
[45] E. Paineau, K. Antonova, C. Baravian, I. Bihannic, P. Davidson, I. Dozov, M. Impéror-Clerc, P. Levitz, A. Madsen, F. Meneau, L.J. Michot, J. Phys. Chem. B 113 (2009) 15858–15869.
[46] I. Dozov, E. Paineau, P. Davidson, K. Antonova, C. Baravian, I. Bihannic, L.J. Michot, J. Phys. Chem. B 115 (2011) 7751–7765.
[47] J.-Ch.P. Gabriel, C. Sanchez, P. Davidson, J. Phys. Chem. 100 (1996) 11139–11143.